JGR Oceans

RESEARCH ARTICLE
10.1029/2019JC016016

Tidal Effects on the Surface Water Cooling Northeast of Hainan Island, South China Sea

Yineng Li[1,2,3,4], Enrique N. Curchitser[5], Jia Wang[6], and Shiqiu Peng[1,2,3,4]

[1]State Key Laboratory of Tropical Oceanography, South China Sea Institute of Oceanology, Chinese Academy of Sciences, Guangzhou, China, [2]Key Laboratory of Science and Technology on Operational Oceanography, Chinese Academy of Sciences, Guangzhou, China, [3]Southern Marine Science and Engineering Guangdong Laboratory (Guangzhou), Guangzhou, China, [4]Institution of South China Sea Ecology and Environmental Engineering, Chinese Academy of Sciences, Guangzhou, China, [5]Department of Environmental Sciences, Rutgers University, New Brunswick, NJ, USA, [6]NOAA Great Lakes Environmental Research Laboratory, Ann Arbor, MI, USA

Key Points:
- Two surface cooler water centers occur in the regions east of Wenchang city and east of the Qiongzhou Strait in summer
- The inhomogeneous tidal mixing between the coastal and open ocean changes the circulations in the northwestern SCS
- On the interannual scale, the cooling induced by tides weakens during La Niña years, while significantly enhances during El Niño years

Correspondence to:
S. Peng,
speng@scsio.ac.cn

Citation:
Li, Y., Curchitser, E. N., Wang, J., & Peng, S. (2020). Tidal effects on the surface water cooling northeast of Hainan Island, South China Sea. *Journal of Geophysical Research: Oceans*, *125*, e2019JC016016. https://doi.org/10.1029/2019JC016016

Received 25 DEC 2019
Accepted 12 SEP 2020
Accepted article online 17 SEP 2020

Abstract Using a 3-D high-resolution ocean model, this paper explores the mechanisms that cause surface and subsurface water cooling northeast of Hainan Island during summer. Results show that two cooling centers in the regions east of Wenchang city and east of the Qiongzhou Strait occur when tides are included in the model. The cooling is primarily caused by large-scale changes in the circulation in the northwestern South China Sea (SCS) through anomalous horizontal pressure gradients caused by inhomogeneous tidal mixing between the near-shore and off-shore regions. East of Wenchang city, the offshore tidal currents induce upwelling that brings the near-bottom cold water to the subsurface. For the region east of the Qiongzhou Strait, the tidally induced westward anomalous currents suppress the warm water transport from Qiongzhou Strait, resulting in a compensating intrusion of cold water from surrounding regions. In addition to the large-scale circulation changes, the local tidal mixing also contributes to the subsurface water cooling east of the Qiongzhou Strait by mixing near-bottom cold water with subsurface waters. Interannually, the cooling weakens or intensifies during different (cold or warm) phases of the El Niño–Southern Oscillation (ENSO) events. This is attributed to variability in surface forcings and large-scale circulation associated with different phases of ENSO leading to changes in stratification, which changes the tidally induced horizontal pressure gradient in the northwestern SCS.

Plain Language Summary The surface water cooling around the eastern and northern coast of Hainan Island is one of the strongest in the South China Sea (SCS). During summer, strong surface water cooling occurs northeast of the island, which is associated with tidal effects. Variable tidal mixing between the coastal region and the open ocean changes the pressure gradient, which results in significant changes in the circulation in the northwestern SCS leading to cooling of the surface waters. On the interannual scale, the sea water cooling induced by tides northeast of Hainan Island weakens (enhances) during the cold (warm) phases of El Niño–Southern Oscillation (ENSO) events.

1. Introduction

In coastal oceans, upwelling is an important dynamical process, which lifts cold, nutrient-rich, waters from the deep to the surface and subsurface (Ekman, 1905). The interseasonal or interannual variability in upwelling can significantly affect biological productivity (e.g., Bakun et al., 1998). During summertime, coastal upwelling is one of the most important phenomena in the northern South China Sea (SCS), where wind and upper-ocean variability is dominated by the East Asian monsoon system (Su, 2004; Wyrtki, 1961; Xie et al., 2003).

The upwelling system around the eastern coast of Hainan Island is one of the strongest in the SCS (Guo et al., 1998), and because of the considerable impacts on the local ecosystem (Chia et al., 2001, Song et al., 2012), its dynamics and variability have gained increased attention. The strong upwelling around the eastern coast of Hainan Island occurs predominantly during the months of June to August due to the steady and strong southerly wind (Guo et al., 1998; Jing et al., 2009, 2011; Wang et al., 2015; Zeng et al., 2014). Both wind-driven Ekman transport and Ekman pumping were suggested to be the primary mechanisms for the upwelling (Guo et al., 1998; Jing et al., 2009, 2011). Additionally, the interannual variations in upwelling are dominated by the East Asia summer monsoon (Wang et al., 2006) and large-scale circulation in the

northern SCS (Li et al., 2012; Su et al., 2013). Recently, the upwelling system around the eastern coast of Hainan Island has been classified into two parts (e.g., Li et al., 2012): upwelling east of the island and upwelling or surface cooling, northeast of the island. Both observational and reanalysis data of sea surface temperature (SST) reveal that surface cooling occurs frequently in this region (Bai et al., 2016; Jing et al., 2015; Li et al., 2012). Different from the upwelling east of Hainan Island, the surface cooling that occurs northeast of the island is not a classic wind-driven coastal upwelling regime—in addition to wind forcing, eddies and tides were also reported as important factors affecting water temperature (Bai et al., 2016; Li et al., 2012; Song et al., 2012; Yu, 1987). Bai et al. (2016) used the Regional Ocean Modeling System (ROMS) to investigate the low-SST event in the summer of 2010. They found that tides play a critical role in the formation of the lower SST core northeast of Hainan Island. In addition, the cross-isobar forces induced by the interaction of currents and topography play an important role in the upwelling intensification east and northeast of Hainan Island (Lin et al., 2016). To date, most model simulations of upwelling in this region either do not include tides (e.g., Jing et al., 2009, 2011; Li et al., 2012; Su & Pohlmann, 2009; Su et al., 2011, 2013) or did not consider the seasonally distinct impacts of the tides (Bai et al., 2016; Wang et al., 2015). Moreover, previous studies have shown that the long-term variability in the upwelling systems in the SCS are typically associated with the El Niño–Southern Oscillation (ENSO) (Hu & Wang, 2016; Xie et al., 2003). However, the interannual variability in surface cooling northeast of Hainan in summer associated with ENSO has not yet been investigated.

In this paper, satellite remote sensing SST data and high-resolution model simulations are used to investigate the seasonal tidal effects on the surface and subsurface cooling northeast of Hainan Island, as well as the interannual variability associated with various phases of ENSO events. This paper is organized as follows: Section 2 gives a description of the satellite data and model configuration. The surface features of cooling as well as seasonal variations in the tidal effects on the cooling are shown in section 3. Section 4 presents the interannual variability in the tidal effects on the cooling associated with different phases of ENSO events, as well as the corresponding dynamical analysis. A summary is given in section 5.

2. Data and Methodology

2.1. Satellite Data

The satellite data used in this study include SST reanalysis with 25-km resolution from the Advanced Very High-Resolution Radiometer (AVHRR) and daily averaged Moderate Resolution Imaging Spectroradiometer (MODIS_Aqua) level 3 gridded data with a 4-km resolution. The MODIS data are provided by the Jet Propulsion Laboratory (JPL) of the National Aeronautics and Space Administration (NASA), which captures SST signals in 36 spectral bands ranging in wavelengths from 0.4 to 14.4 μm and at varying spatial resolutions (2 bands at 250 m, 5 bands at 500 m, and 29 bands at 1 km), providing complete global coverage of the Earth every 1 to 2 days (Ocean Biology Processing Group, 2014).

2.2. Model Description and Configuration

In this study, the 2004 version of the 3-D Princeton Ocean Model (POM) is used (Blumberg & Mellor, 1987; Mellor, 2004). The POM uses the 2.5-order turbulence closure scheme of Mellor and Yamada (1982) for turbulence viscosity and diffusivity calculations.

The model domain covers all of Hainan Island, as well as the Beibu Gulf in the northwestern SCS from 13°N to 23°N and 105°E to 115°E (as shown in Figure 1), with a horizontal resolution of 1/30° (approximately 3.6 km) and 47 vertical layers in sigma (terrain following) coordinates refined in both the upper and near-bottom parts of the ocean. We use the General Bathymetric Chart of the Oceans (GEBCO_08) bathymetry data (http://www.gebco.net/) with a high resolution of 30 arc seconds. The minimum depth of the model is set to 10 m in the coastal region, according to the physical stability criterion of the global stability given by Wang (1996): $h_{min}+\varsigma_{max} > 0$, where h_{min} is the minimum water depth and $\varsigma_{max}$is the maximum water elevation, which may be caused by strong (gusty) winds along the coast in some regions of the East China Sea and northern SCS. The barotropic and baroclinic time steps are set to 6 and 120 s, respectively. The open boundaries are forced by the monthly mean Simple Ocean Data Assimilation (SODA3.3.1) reanalysis (Carton et al., 2018). The radiation boundary condition is implemented to obtain normal advection of variables at the open boundaries (Mellor, 2004).

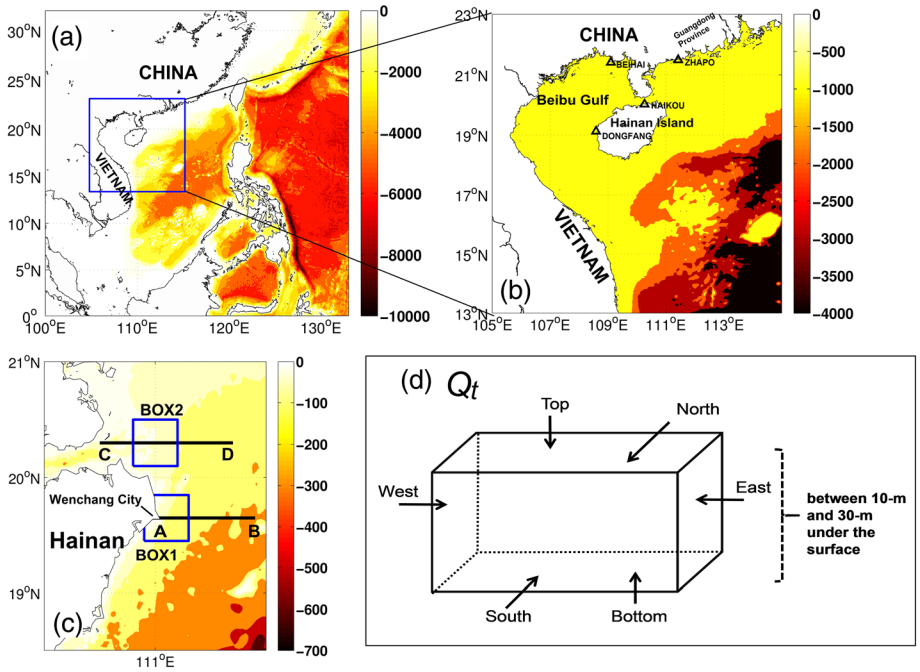

Figure 1. (a) The location and (b) bathymetry (units: m) of the model domain (the triangles are the tide gauges for model validation), (c) the locations of cuboids BOX 1 and BOX 2 and transects AB and CD, and (d) a schematic diagram illustrating the temperature advection fluxes (*Qt*) into the cuboid from different directions.

The initialization procedure of the model includes two steps. First, the POM is integrated for 20 years from zero velocity and the climatological temperature and salinity of the World Ocean Atlas 2013 (WOA13) in January (Locarnini et al., 2013). The surface forcings in this step are from the data of climatological wind stress, heat flux, and shortwave radiation flux, which are obtained from the National Center for Atmospheric Research (NCAR)/National Center of Environment Prediction (NCEP) reanalysis (Kalnay et al., 1996). This process is generally referred to as the "spin-up," which aims to obtain a quasi-equilibrium state in the upper ocean (Zhang & Qian, 1999). Second, the model is integrated from 1 January 1980 to 31 December 2010, while the outputs from 1981 to 2010 are used for analysis. The 6-hourly surface winds are from two data sets: the 2.5° resolution NCEP/NCAR reanalysis from 1981 to 1987 and the high-resolution (0.25°) cross-calibrated multiplatform (CCMP) Ocean Surface Wind Vector Analysis from 1988 to 2010, which was obtained using a variational analysis method (VAM) (Atlas et al., 2011). The CCMP data set includes cross-calibrated satellite winds derived from SSM/I, SSMIS, AMSR-E, TRMM TMI, QuikSCAT, SeaWinds, WindSat, and other satellite instruments as they become available from remote sensing systems (RSSs; Atlas et al., 2011). Other meteorological forcing data, including air temperature, humidity, E-P (evaporation minus precipitation), and shortwave radiation flux are also extracted from the NCEP/NCAR reanalysis. To investigate the tidal effects, two 30-year model runs with and without tides in the boundary are implemented, which are denoted as TIDE and NO_TIDE, respectively. The tides are incorporated into the model open boundaries with eight tidal constituents (M2, S2, N2, K2, K1, O1, P1, and Q1) from the OTPS (Oregon State University Tidal Prediction Software) (Egbert & Erofeeva, 2002).

2.3. Composite Analysis

To investigate the tidal effects on sea water cooling northeast of Hainan Island in warm (El Niño) or cold (La Niña) phases of ENSO events, a composite analysis is used. The El Niño events are selected based on the NOAA criterion that the Ocean Niño Index (ONI) should be greater than or equal to 0.5°C for a period of at least 5 consecutive and overlapping 3-month periods. In this study, we only consider those El Niño events with warm sea surface centers located in the eastern Pacific and neglect those with warm sea surface centers located in the central Pacific (the tidal effects for the latter are similar to those for the former, though much

Table 1
The Transport of the Qiongzhou Strait (Sv)

	Winter	Spring	Summer	Autumn
NO TIDE	−0.25	0.028	0.20	−0.26
TIDE	−0.21	−0.084	−0.018	−0.20
Shi et al. (2002)	−0.2–−0.4		−0.1–−0.2	
Zhu et al. (2014, 2015)	/	−0.021–−0.111/−0.044	/	/

weaker) (e.g., see Kug & Jin, 2009; Ren & Jin, 2011; Yeh et al., 2009; Yu et al., 2012); thus, according to the table of Yu et al. (2012) and the time series of ONI, four strong warm phase (El Niño) events (1982/1983, 1986/1987, 1997/1998, and 2006/2007) and eight significant cold phase (La Niña) events (1988/1989, 1995/1996, 1998/1999, 1999/2000, 2000/2001, 2005/2006, 2007/2008, and 2008/2009) are chosen for the composite analysis. Here the ocean state in the summer (such as 1998, the strongest El Niño of the twentieth century) is used to investigate the impact of ENSO events in the preceding winter (1997/1998), according to a recent research result that the summer SST in the SCS is correlated with ENSO in the preceding winter (Yang et al., 2015). In this study, the Student's t distribution is used to determine the statistical significance between means of two samples (Bai et al., 2012).

2.4. Model Validation

The tidal simulation from 1 January 1995 to 31 December 1997 is validated against observations from four tide gauge stations (ZHAPO, BEIHAI, DONGFANG, and HAIKOU, as shown in Figure 1b) from the research quality data set of the Joint Archive for Sea level (JASL; Caldwell et al., 2015), which is provided by the University of Hawaii Sea-level Center (UHSLC). Except for HAIKOU, the biases of the amplitudes and phases of the four main constituents are less than 10%. The biases of diurnal tides (K1 and O1) at HAIKOU are approximately 10%, while those of the semidiurnal tides are approximately 20%. However, the amplitudes of the semidiurnal tides at HAIKOU are relatively small; thus, the overall biases of HAIKOU are still comparable to those of other tide gauges. The correlation coefficients between the modeled outputs and observations are 0.987, 0.997, 0.995, and 0.995 for ZHAPO, BEIHAI, DONGFANG, and HAIKOU, respectively. Accounting for the errors caused by the relatively coarse topographic data, the skill of the model in the tidal simulation is acceptable.

The modeled transport of the Qiongzhou Strait is shown in Table 1. Based on the observations from Shi et al. (2002), the flow in the Qiongzhou Strait is westward year round, with volume transports of approximately 0.2–0.4 Sv during winter and spring and 0.1–0.2 Sv during summer and autumn. Recently, observations from Zhu et al. (2014, 2015) show that the transport of the Qiongzhou Strait is approximately −0.021– −0.111 Sv in spring (negative values refer to the westward transport). The model with tidal forcings simulates a transport of −0.084 Sv in spring and −0.21 Sv in winter, which is close to the observations, indicating that the model run with tidal forcings is reliable. However, the model without tidal forcings cannot reproduce the westward transport during spring and summer, suggesting that tides play a key role in driving the circulation around Qiongzhou Strait. Therefore, tidal effects should be considered when modeling this region.

Table 2
The Tidal Harmonic Constants (M2, S2, K1, and O1) of Model Outputs (Data Without Parenthesis) and Tide Gauge Observations (With Parenthesis) in the Location of Four Tide Gauges (Referred in Figure 1); Am, Ph, and CC Refer to the Amplitude (unit: m), Phase (unit: °), and Correlation Coefficient, Respectively

	M2_Am	M2_Ph	S2_Am	S2_Ph	K1_Am	K1_Ph	O1_Am	O1_Ph	CC
ZHAPO	0.64 (0.65)	100.4 (89.7)	0.27 (0.29)	132.1 (122.7)	0.43 (0.42)	211.1 (212.3)	0.37 (0.36)	169.9 (167.8)	0.987
BEIHAI	0.50 (0.53)	337.8 (332.4)	0.10 (0.10)	22.1 (22.9)	0.94 (1.00)	350.9 (352.8)	0.97 (1.05)	291.8 (290.5)	0.997
DONGFANG	0.19 (0.20)	220.3 (218.6)	0.06 (0.06)	264.8 (270.3)	0.52 (0.57)	324.3 (327.3)	0.61 (0.67)	272.6 (271.5)	0.995
HAIKOU	0.18 (0.24)	62.5 (51.1)	0.11 (0.15)	120.0 (111.1)	0.37 (0.41)	338.1 (350.3)	0.50 (0.55)	289.3 (294.5)	0.995

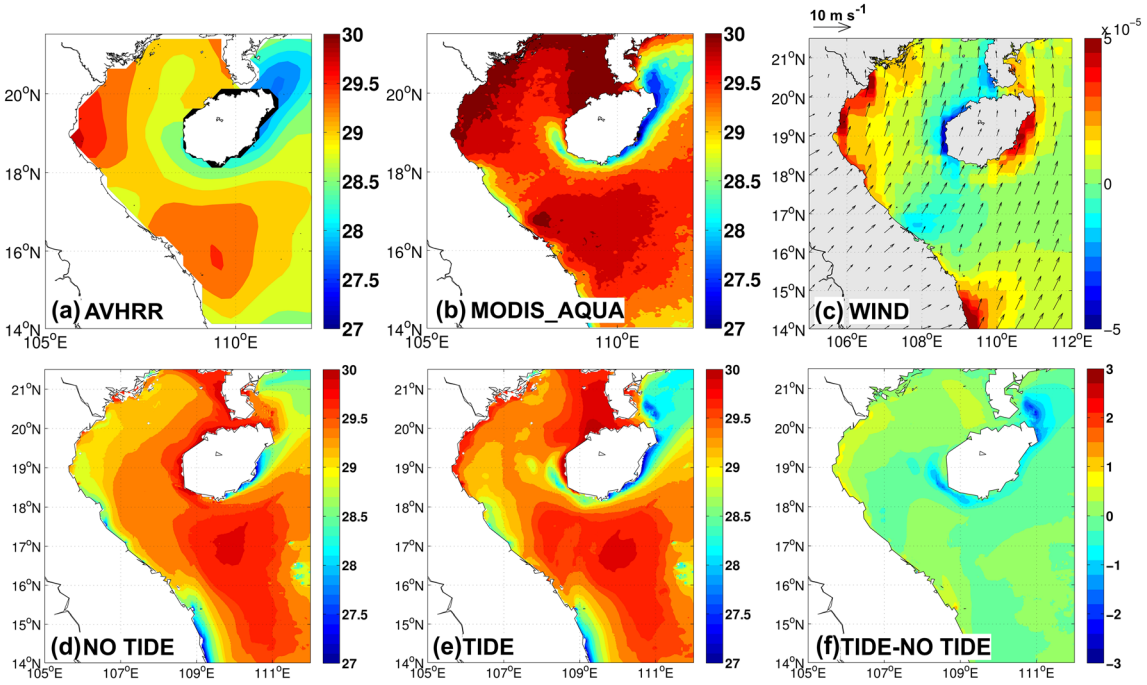

Figure 2. The climatological monthly mean SST (units: °C) in July from (a) NOAA AVHRR and (b) MODIS_AQUA, (c) the climatological monthly mean wind field superimposed by the wind stress curl (units: 10^3 N·m^{-3}) from the CCMP data set (only the wind stress curl over the ocean grids is shown), and the modeled SST (units: °C) from experiments (d) NO_TIDE, (e) TIDE, and (f) their differences (TIDE minus NO_TIDE).

3. The Features and Seasonal Variations in Tidal Effects

3.1. The Features of Surface Cooling Northeast of Hainan Island

Cooler water can be inferred from SSTs measured by satellites in the northern SCS (e.g., Jing et al., 2009, 2011; Wang et al., 2015; Zeng et al., 2014). We use two climatological monthly mean SST data sets, which were created using daily data from 1982 to 2010 (AVHRR) and from 2003 to 2017 (MODIS). The climatological monthly mean SSTs from satellite data in July (Figures 2a and 2b) show that the lower-SST centers can be observed northeast of Hainan Island, as well as east of the island. Moreover, compared with AVHRR, MODIS provides more details in the coastal region due to its higher spatial and temporal resolutions. For example, there is a higher SST inside the Qiongzhou Strait. Obviously, the model with tides can reproduce the satellite-observed lower-SST centers northeast of Hainan Island, as well as the higher SST inside the Qiongzhou Strait (Figure 2e). In July, southwesterly winds are prevalent with a large positive wind stress curl on the eastern coast of Hainan Island (Figure 2c), which induces strong upwelling east of Hainan Island through Ekman transport and Ekman pumping in both TIDE and NO_TIDE cases (Figures 2d and 2e). However, the lower SST centers northeast of Hainan Island occur only when tides are included (Figures 2e and 2f). These results imply that in July, tides are essential to the generation of lower-SST centers northeast of the island.

3.2. Seasonal Variations in Tidal Effects

Figure 3 shows the seasonal variations in tidal effects on currents and sea subsurface temperature northeast of Hainan Island. The inclusion of tides changes the currents around Qiongzhou Strait significantly throughout the year, while the tidal effects on temperature vary seasonally. In winter (Figures 3a, 3c, and 3e), when sea temperature is relatively low, the difference between TIDE and NO_TIDE around Hainan Island is marginal. In summer (Figures 3b, 3d, and 3f), significant cooling induced by tides is found northeast (as well as southwest) of Hainan Island. The results indicate that tidal effects on the sea temperature northeast (as well as southwest) of Hainan Island have seasonal variations.

The seasonality in currents with and without tidal forcings can be further investigated with the sea surface height (SSH) and depth-averaged currents, as shown in Figure 4. When tides are excluded in the model,

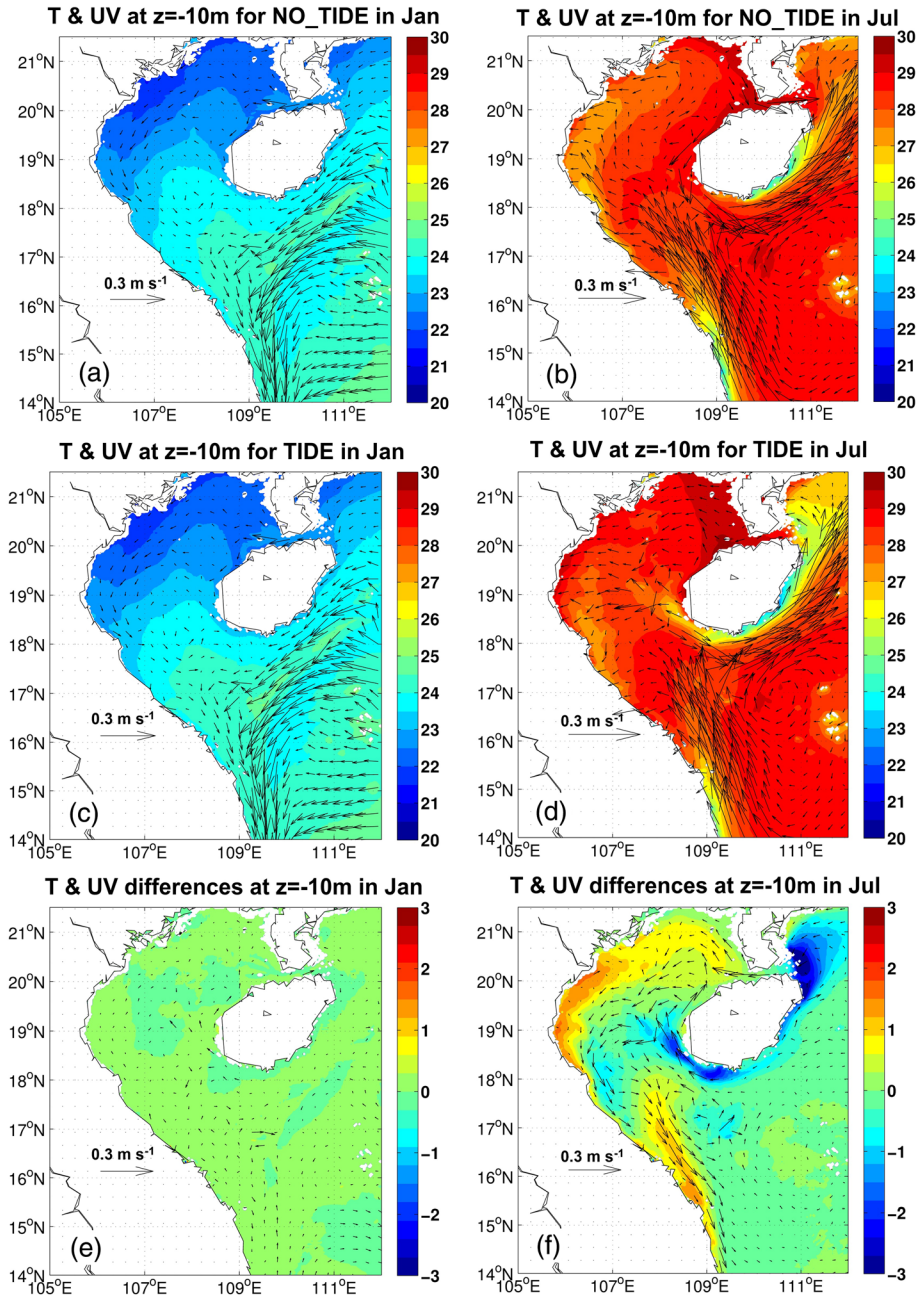

Figure 3. The sea temperature (units: °C) superimposed by currents at $z = -10$ m from NO_TIDE (top panels) and TIDE (middle panels) and the differences (bottom panels) between TIDE and NO_TIDE in (a, c, and e) January and (b, d, and f) July.

the main circulation in the northwestern SCS follows the isolines of SSH, which are parallel to the isobaths of the continental shelf (Figures 1, 4a, and 4b). In summer, the SSH in the coastal region is considerably lower than that in the open ocean region, leading to an onshore cross-isobath pressure gradient in the northwestern SCS. This pressure gradient drives the northeastward circulation along coastal regions of the Guangdong Province and eastern Hainan Island, as well as the eastward currents in the Qiongzhou Strait during summer, according to the geostrophic balance (Figure 4b). The pressure gradient reverses in winter, resulting in a reversal of the circulation pattern in the northwestern SCS (Figure 4a).

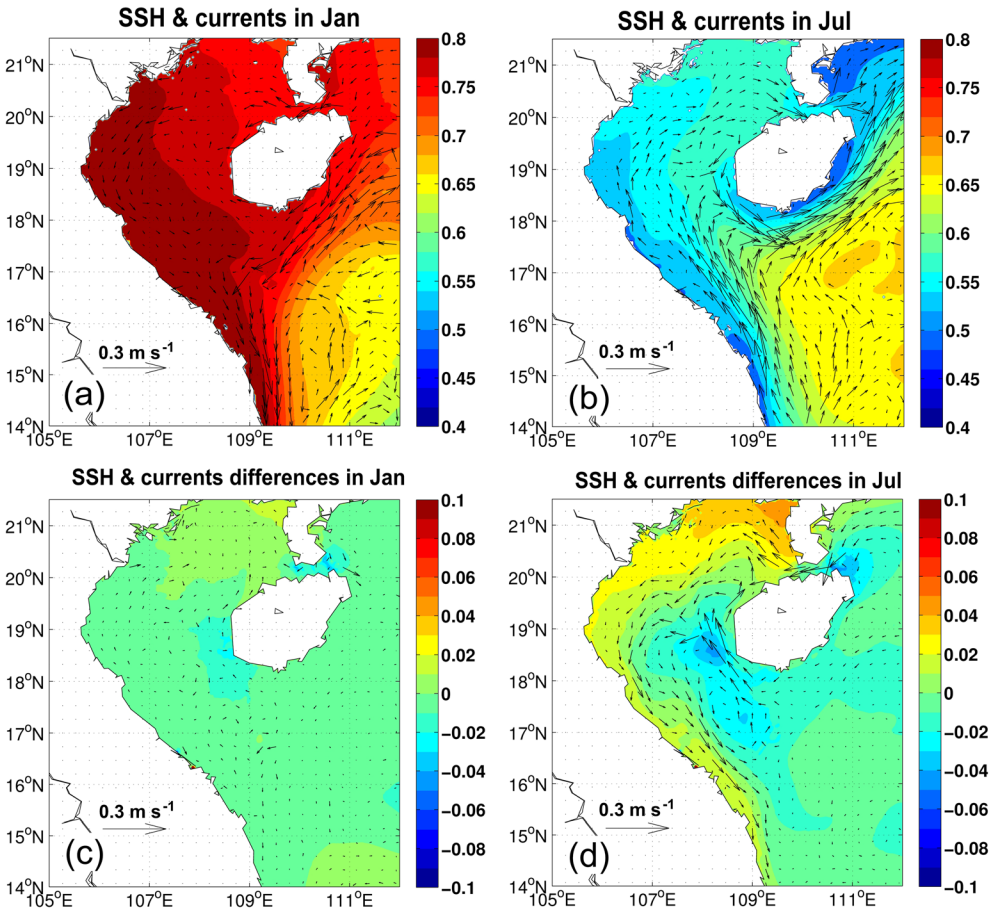

Figure 4. The SSH (units: m) superimposed by depth-averaged currents from NO_TIDE (top panels) and the differences between TIDE and NO_TIDE (bottom panels) in (a, c) January and (b, d) July.

When tides are included in the model, the SSH increases significantly in coastal regions and decreases slightly in offshore regions in summer, whereas the changes in SSH are not significant in winter (Figures 4c and 4d). These changes in SSH in summer result in a pressure gradient from near-shore to offshore regions, causing a reversing anomalous circulation pattern along the Vietnam and Beibu Gulf (as shown in Figure 4d with respect to Figure 4b). Specifically, significant westward current anomalies are induced in the Qiongzhou Strait.

As shown earlier, tidal effects induce two main cooling centers in the regions east of Wenchang city and east of the Qiongzhou Strait in summer. To further investigate the seasonal variations in tidal effects, we examine the vertical distribution of sea temperature and currents along transects AB and CD, respectively (Figures 1, 5, and 6). Along transect AB (east of Wenchang city), the water is well mixed and not stratified in winter. Downwelling occurs in the coastal region due to the onshore currents driven by the strong northeast monsoon winds (Figures 5a and 5c). As a result, the differences in temperature profiles with and without tides are small near the coastal region of Wenchang city (Figure 5e). In summer, strong solar heating and weak winds (i.e., weak mixing) stratify the water column, which can suppress upwelling when tides are excluded from the model. Therefore, coastal upwelling and surface cooling are not significant (Figure 5b). When tides are included, however, strong upwelling and offshore currents are induced with subsurface sea temperatures dropping by more than 2°C (Figures 5d and 5f), which implies that in summer, tides play a key role in driving the offshore currents and upwelling in the region east of Wenchang city.

Unlike transect AB, a seamount separates transect CD into two parts: the Qiongzhou Strait and the region to the east of the strait (Figure 6). When tides are excluded from the model, upper water is well mixed inside the

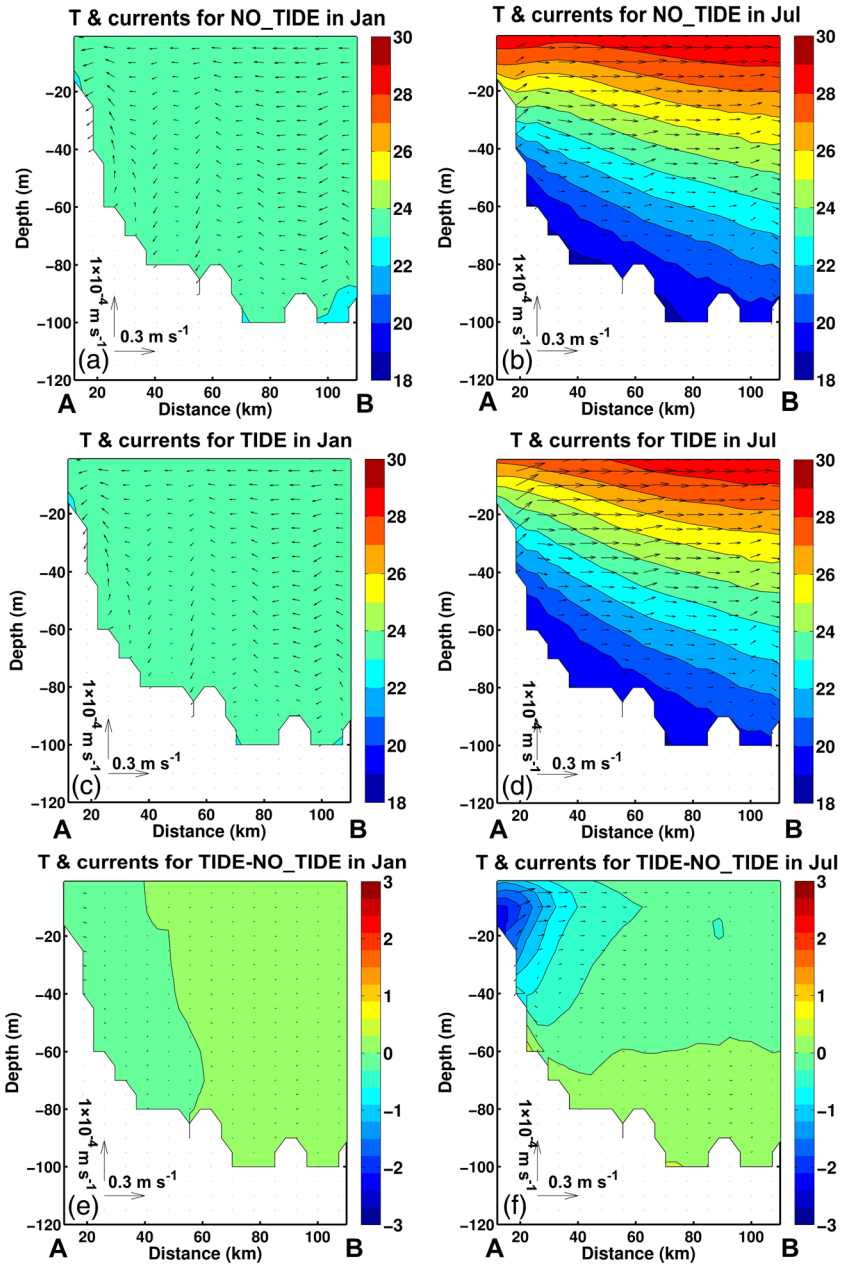

Figure 5. The sea temperature (units: °C) superimposed by currents along transect AB from NO_TIDE (top panels) and TIDE (middle panels) and the differences (bottom panels) between TIDE and NO_TIDE in (a, c, and e) January and (b, d, and f) July.

Qiongzhou Strait throughout the year, while it is well mixed in winter and stratified in summer in the region east of the Qiongzhou Strait (Figures 6a and 6b). Therefore, the temperature profiles are quite different between the inside and outside of the Qiongzhou Strait in summer. In addition, the eastward currents can transport the warmer water into the region east of the strait (Figure 6b). When tides are included in the model, strong westward current anomalies induced by tides suppress the transport of warmer water from the Qiongzhou Strait, leading to a compensation of subsurface cooler water into the region in summer. As a result, a significant temperature reduction of up to 4°C occurs near the eastern edge of the Qiongzhou Strait (Figures 6d and 6f).

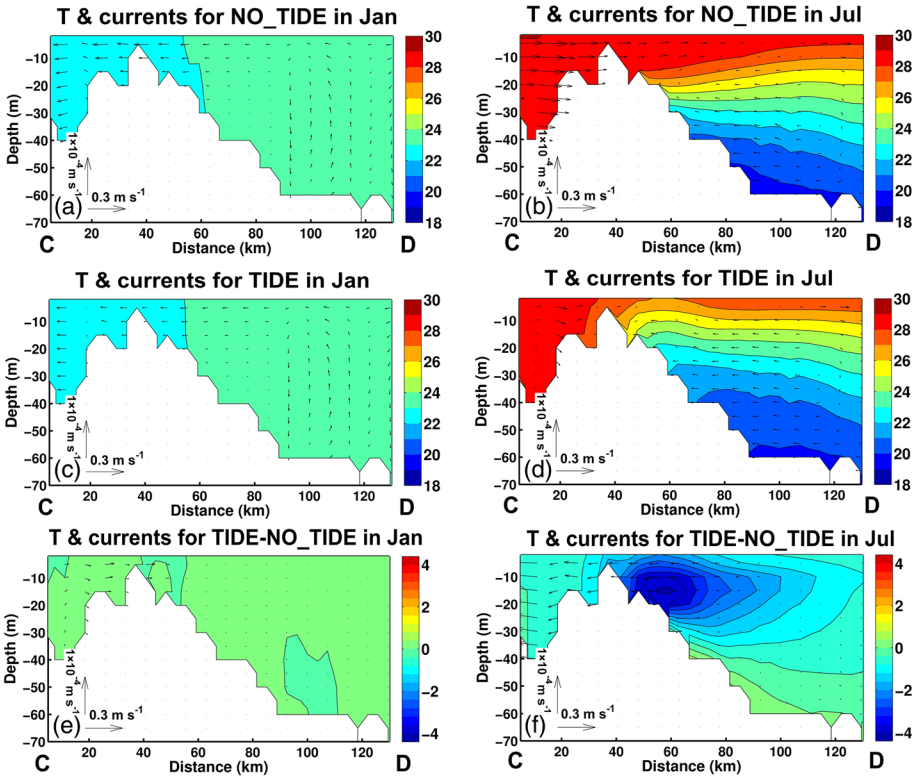

Figure 6. The same as in Figure 5 except for transect CD.

3.3. Dynamical Analysis of Tidal Effects

As shown in section 3.2, tidal effects induce significant mean flow changes northeast of Hainan Island. To investigate how these flow changes affect the subsurface sea temperature northeast of Hainan Island, the time series of temperature advection flux are analyzed for the cuboids of BOX 1 and BOX 2 with vertical depths of 10 to 30 m (as shown in Figure 1). The temperature advection flux is defined as follows:

$$dQ_t = A \cdot U \cdot \left(T_{inflow} - T_{cuboid}\right) \tag{1}$$

where A is the area of each side of the cuboid, U is the velocity, and T_{inflow} and T_{cuboid} are the temperature of the ocean grid in the inflow sides of the cuboid and the temperature of the cuboid, respectively. The positive (negative) value of dQ_t means that higher (lower) temperature water is transported into the cuboid, increasing (decreasing) the temperature of the cuboid. Since we want to trace the source of temperature reduction in the cuboid, here we only consider the situation of $dQ_t < 0$.

Figures 7a and 7b show the time series of differences in sea temperature, offshore velocity, and vertical velocity averaged in the two cuboids of BOX 1 and BOX 2 between TIDE and NO_TIDE. For BOX 1, similar to the results shown in Figure 5, significant anomalies of sea temperature, offshore current, and vertical velocity can be found from late spring to summer when tides are included in the model. The offshore currents (positive x direction velocities) and upwelling velocities (positive vertical velocities) reach their maximum in June and July (approximately days 170 to 200 of the year), corresponding to a maximum temperature reduction. The temperature reduction is mainly caused by cold water advection from the bottom and south sides of cuboid BOX 1 with the existence of tides (Figure 7c). In particular, the temperature advection flux from the bottom side is nearly double that from the south side in most of the summer. These results indicate that the upwelling induced by tides is the main source of temperature reduction in the region of BOX 1.

In the region east of Qiongzhou Strait (BOX 2), however, the mechanism for sea water cooling is different. As shown in Figure 7b, significant temperature reductions induced by tides are accompanied by downwelling (negative vertical velocities) and onshore currents (negative x direction velocities). Further investigation

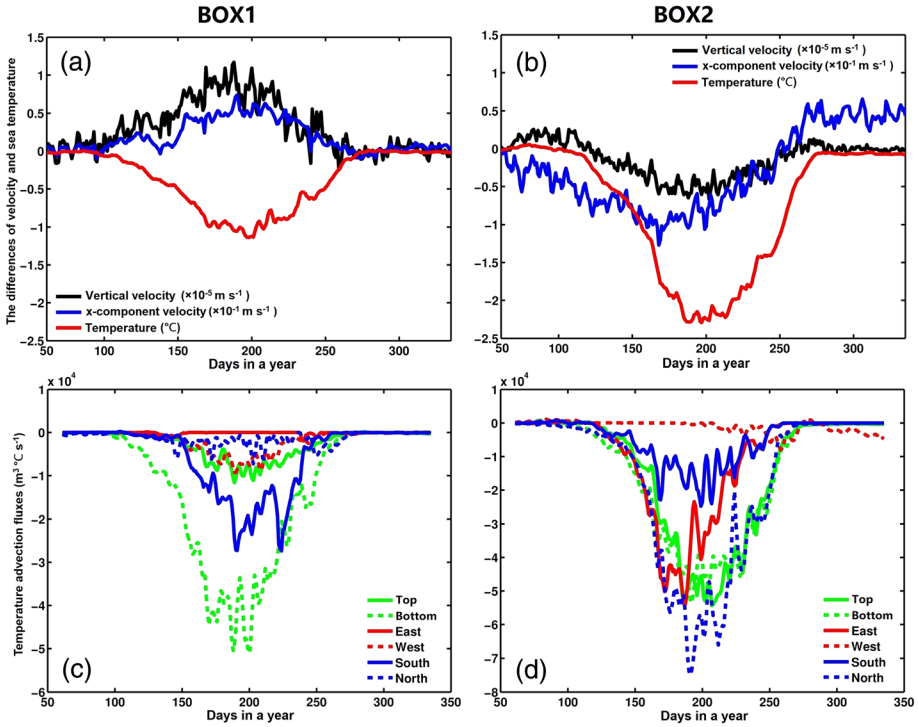

Figure 7. The daily variations in cuboid-averaged differences of vertical velocity (unit: $\times 10^{-5}$ m s^{-1}), x component velocity (unit: $\times 10^{-1}$ m s^{-1}), temperature (unit: °C, top panels) between TIDE and NO_TIDE in cuboids BOX 1 (left panels) and BOX 2 (right panels), and temperature advection flux differences (units: m^3 °C s^{-1}, bottom panels) on each side of the cuboids (as denoted in Figure 1).

of the temperature advection flux in BOX 2 (Figure 7d) indicates that the temperature reductions in the region east of Qiongzhou Strait during summer are mainly attributed to horizontal cold water advection from the north and east sides of BOX 2, in addition to the vertical cold water entrainment from the bottom sides. Notably, the enhancement of near-bottom vertical mixing (tidal mixing) around the cooling region in BOX 2 is much larger than that in BOX 1, as shown in Figure 8. Due to the shearing and temporary divergence induced by strong reciprocating tidal currents, tidal mixing causes significant sea water exchange with negative temperature advection flux from the bottom of the cuboid (BOX 2). Based on Figures 6, 7, and 8b, it can be concluded that the westward currents induced by tides suppress the warmer water transport from the Qiongzhou Strait into the region east of the strait, and then the compensation of cooler water from the surrounding areas combined with the entrainment of bottom cooler water induced by the local tidal mixing reduces the temperature in the region of BOX 2.

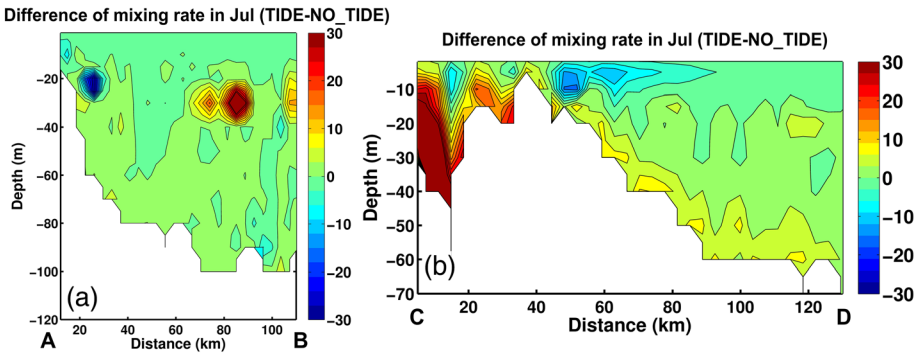

Figure 8. The differences of the vertical mixing rate (units: 10^{-3} m^2 s^{-1}) along transects (a) AB and (b) CD between TIDE and NO_TIDE in July.

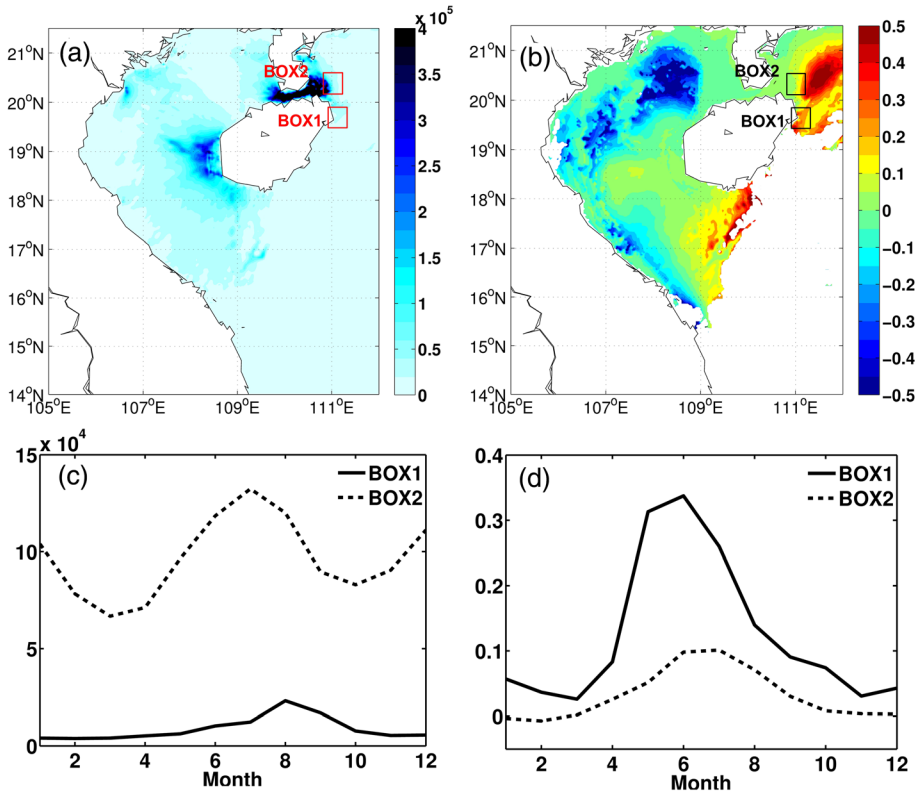

Figure 9. The differences of (a) tidal power for mixing (units: J m^{-2}) between TIDE and NO_TIDE and (b) the ratio (Φ) of upper ocean TIDE-induced potential energy changes (*dPE*) integrated from 0 to 50 m depth to tidal power in July (the values over low tidal power regions are not shown) and the time series of differences of (c) tidal power for mixing (units: J m^{-2}) between TIDE and NO_TIDE and d the ratio (Φ) averaged over BOX 1 and BOX 2.

The previous results indicate that the sea temperature changes in the two regions northeast of Hainan Island are mainly induced by remote tidal mixing, which changes the circulation around Hainan Island. To quantify the effect of remote versus local tidal mixing on the temperature changes in the two regions, we calculate the tidal power for local mixing and the ratio (Φ) of the upper ocean tide-induced potential energy changes (*dPE*) to tidal power. The bottom friction power (BFP; unit: J/m^2) can be defined as follows:

$$BFP = a\int_0^T \rho_0 C_z |U|^3 dt, \tag{2}$$

where ρ_0 is the reference density of seawater, $C_z$is the bottom drag coefficient, and U is the hourly current speed. T is the time of the model integration, while a is the local dissipation efficiency chosen as 0.3 (Laurent et al., 2002). Following the method of Sun et al., 2015, the ratio (Φ) is defined as follows:

$$\Phi = dPE/tidal\ power = \frac{\int_D^0 \rho_{TIDE} gz dz - \int_D^0 \rho_{NOTIDE} gz dz}{BFP_{TIDE} - BFP_{NOTIDE}} \tag{3}$$

where g is gravity, z is the depth in conventional Cartesian coordinates, $D = H + \eta$ is the total water depth, $H(x, y)$ is the bottom topography, $\eta(x, y, t)$ is the surface elevation, and ρ_{TIDE} and ρ_{NOTIDE} are the densities of the model runs TIDE and NOTIDE, respectively. A large value of the ratio means that the tide-induced *PE* changes are mainly forced by remote tidal mixing and vice versa.

As shown in Figure 9a, the regions with large tidal power are mainly located in Qiongzhou Strait, west and southwest of Hainan Island, and coastal area in the northern Beibu Gulf. Therefore, the tidal power in BOX 2 is nearly 10 times that in BOX 1 during summer (Figure 9c). However, the ratio in BOX 1 is much larger than that in BOX 2 (Figures 9b and 9d). This difference indicates that remote tidal mixing dominates the tidal *PE*

changes in the region east of Wenchang city, while both remote and local tidal mixing are vital to the *PE* changes in the region east of the Qiongzhou Strait. In addition, as shown in Figures 3f and 4d, the tide-induced higher SSH in the nearshore regions of northwestern SCS drives westward currents along the strait, which not only suppresses warmer water transporting from Qiongzhou Strait to the region northeast of Hainan Island but also transports the warmer water into the region west of the strait. Therefore, the tide-induced westward currents along the strait results in a decrease (increase) of density and thus a negative (positive) PE/ratio west (east) of the strait (Figure 9b). To further investigate how tides influence the surface and subsurface cooling by changing the mean flow, we perform an analysis on the corresponding dynamical processes using the following vertically integrated momentum equations (Mellor, 2004):

$$\begin{aligned}\frac{\partial uD}{\partial t} = &\underbrace{-\frac{\partial u^2 D}{\partial x} - \frac{\partial uvD}{\partial x} + \tilde{F}_x + G_x + fvD - gD\frac{\partial \eta}{\partial x}}_{AD} \quad \overline{COR} \quad \overline{PBT} \\ &\underbrace{-\frac{gD}{\rho_0}\int_{-1}^{0}\int_{\sigma}^{0}\left[D\frac{\partial \rho'}{\partial x} - \frac{\partial D}{\partial x}\sigma\frac{\partial \rho'}{\partial \sigma}\right]d\sigma' + \langle wu(0)\rangle + \langle wu(-1)\rangle}_{PBC} \quad \overline{WS} \quad \overline{BOT}\end{aligned} \tag{4}$$

and

$$\begin{aligned}\frac{\partial uD}{\partial t} = &\underbrace{-\frac{\partial v^2 D}{\partial x} - \frac{\partial uvD}{\partial x} + \tilde{F}_y + G_y + fuD - gD\frac{\partial \eta}{\partial y}}_{AD} \quad \overline{COR} \quad \overline{PBT} \\ &\underbrace{-\frac{gD}{\rho_0}\int_{-1}^{0}\int_{\sigma}^{0}\left[D\frac{\partial \rho'}{\partial y} - \frac{\partial D}{\partial y}\sigma\frac{\partial \rho'}{\partial \sigma}\right]d\sigma' d\sigma\langle wu(0)\rangle + \langle wu(-1)\rangle}_{PBC} \quad \overline{WS} \quad \overline{BOT}\end{aligned} \tag{5}$$

where x, y, and z are the conventional Cartesian coordinates; σ is the sigma coordinate ranging from $\sigma = 0$ at the sea surface to $\sigma = -1$ at the bottom, and ρ is the potential density, with subscripts "0" and "′"representing its reference and perturbation, respectively. F_x and F_y are the horizontal viscosity and diffusion terms, while G_x and G_y are the dispersion terms; the details of F and G are available in Mellor (2004). Terms 1 to 6 on the right-hand side of Equations 4 and 5 refer to nonlinear advection and diffusion (AD: $F + G$), Coriolis force (COR), barotropic pressure gradient (PBT), baroclinic pressure gradient (PBC), surface wind stress (WS), and bottom friction stress (BOT), respectively. Notably, the wind forcing is the same for the TIDE and NO_TIDE experiments, and thus, the differences in WS are negligible. Here the negative COR term in the y direction momentum equation refers to the offshore currents (eastward) in the region and vice versa.

Similar to the tidal power shown in Figure 9a, the mixing rate associated with tides is much higher in the coastal regions of the Beibu Gulf and Qiongzhou Strait than that in offshore regions (Figure 10a). The inhomogeneous changes in the mixing rate, along with the well-stratified upper ocean in offshore regions in summer, induce the baroclinic pressure gradient from the shallow region to the open ocean (Figure 10b; Li et al., 2018), which induces westward currents along the Qiongzhou Strait, southward currents along the Vietnam coast and cyclonic circulation in the Beibu Gulf (Figure 4d). This mechanism is schematically illustrated in Figure 11. Sea water is well stratified in summer in the northern SCS. The shearing of tidal currents induces strong tidal mixing around the bottom boundary layer, which can change the upper ocean stratification in shallow regions. Then, the inhomogeneous change in water density in the upper ocean induces the baroclinic pressure gradient from the shallow region to the open ocean, which forces circulation changes in the Beibu Gulf and around Hainan Island. Here the stratification of the upper ocean (stratification without tidal mixing) is a key factor in the tidal effects on circulation changes and temperature in these regions.

Figures 10c and 10d show the temporal evolution of differences in each term in Equation 5 between TIDE and NO_TIDE averaged in climatological monthly mean and over BOX 1 or BOX 2. This figure reveals that the two terms, pressure gradient and Coriolis force, dominate the tide-induced changes in all terms and

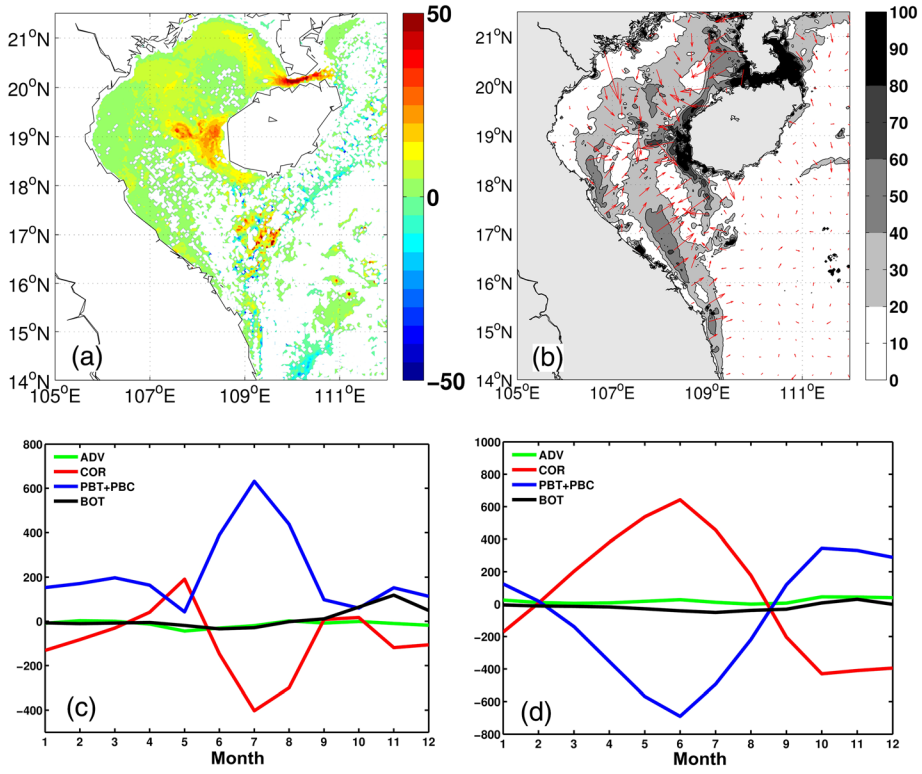

Figure 10. The differences of (a) vertical mixing rate (units: 10^{-3} m^2 s^{-1}) averaged from 10 to 30 m depth and (b) pressure gradient (vectors, (PBT + PBC)/D, units: S^{-2}) in the momentum equation between TIDE and NO_TIDE in July and the differences of each term (units: m s^{-2}) of the momentum equation in the *y* direction between TIDE and NO_TIDE averaged over (c) BOX 1 and (d) BOX 2.

balance each other for both BOX 1 and BOX 2. For BOX 1 (Figure 10c), the magnitudes of positive (northward) pressure gradient anomalies and negative (southward) Coriolis force anomalies increase with the setup of upper ocean stratification in late spring and reach their maxima in July. It implies that the lower SSH east of the Qiongzhou Strait, induced by the westward currents, forces the positive pressure gradient anomalies from east of Wenchang city to east of the Qiongzhou Strait (Figures 4d and 10b). As a result, the offshore (eastward) currents following the geostrophic balance favor upwelling on the eastern coast of Wenchang city (Figure 7a). For BOX 2 (Figure 10d), the signs of these two dominating terms in summer are opposite to those for BOX 1, suggesting onshore (westward) currents in the region east of the Qiongzhou Strait (Figure 7b). The onshore currents do not favor upwelling occurrence but suppress the eastward transport of warm water from the strait, resulting in cooler water advection from the surrounding regions (Figures 3f and 4d). The above analysis indicates that the inhomogeneous tidal mixing in well-stratified water plays a key role in the formation of the subsurface cool water centers east of Wenchang city and east of the Qiongzhou Strait by changing the horizontal pressure gradient and, thus, the large-scale circulations in the northwestern SCS. For the region east of Wenchang city, the tide-induced offshore currents facilitate upwelling that brings near-bottom cold water to the subsurface. For the region east of the Qiongzhou Strait, the tide-induced westward anomalous currents suppress warm water transport from the strait, which results in the compensation of cold water from the surrounding regions. In addition to the tide-induced

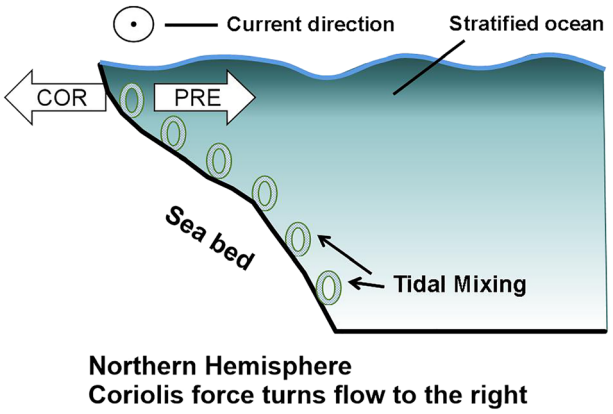

Figure 11. A schematic diagram illustrating how the tidal mixing changes impact the currents in the northwestern SCS in summer (COR and PRE refer to the Coriolis and pressure gradient, respectively).

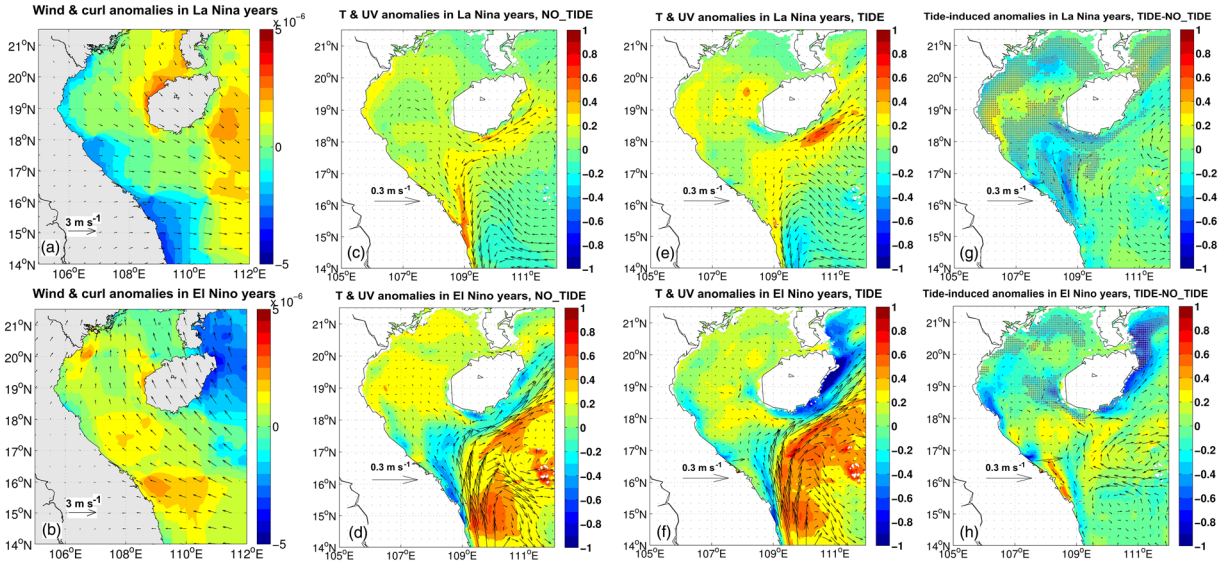

Figure 12. The monthly mean anomalies in July against climatology (30-year mean) of (a, b) 10-m wind (vectors, units: M s^{-1}), wind stress curl (color, units: 10^3 N·m^{-3}), the simulated sea temperature (units: °C) and current anomalies (units: m s^{-1}) at z = −10 m from (c, d) NO_TIDE and (e, f) TIDE, and (g, h) the differences between TIDE and NO_TIDE during the cold phase (La Niña, top panels) and warm phase (El Niño, bottom panels) of ENSO events. Shaded area with dots indicates that differences between TIDE and NO_TIDE are significant above the 95% confidence level).

change in the large-scale circulations (effects of remote tidal mixing), the local tidal mixing also contributes to the subsurface sea water cooling east of the Qiongzhou Strait by mixing the relatively cold near-bottom water with subsurface water.

4. Interannual Variation in Tidal Effects Associated With Different Phases of ENSO Events

Previous studies show that ENSO events have an impact on the thermodynamic processes in the SCS (Chang et al., 2008; Fang et al., 2006; Liu et al., 2014; Wu et al., 1998; Yang & Wu, 2012), as well as on the long-term variabilities in upwelling systems in the SCS (Hu & Wang, 2016; Xie et al., 2003). The anomalies of the monthly mean 10-m wind and wind stress curl in July for cold (La Niña) and warm (El Niño) phases of ENSO events are shown in Figures 12a and 12b. Compared with the climatological wind and wind stress curl shown in Figure 2c, northwesterly wind anomalies (favorable downwelling) and slight positive wind stress curl anomalies occur on the northeastern coast of Hainan Island during the cold phase of ENSO (Figure 12a). As a result, the sea temperature northeast of Hainan Island increases slightly when tides are excluded from the model. During the warm phase of ENSO, the combined effects of intensified southeasterly wind and weaker wind stress curl northeast of Hainan Island induce a slight temperature decrease in the region east of Wenchang city, while the eastward current anomalies in Qiongzhou Strait transport warmer water in the region east of the strait and cause a slight increase in sea temperature.

It is interesting that the anomalies vary significantly with different phases of ENSO events when tides are included in the model (Figures 12g and 12h). Here the anomalies of tidal effects are defined as the differences between tidal changes in ENSO years (e.g., T_{TIDE}-T_{NO_TIDE} averaged during El Niño or La Niña years) and tidal changes in climatology (i.e., T_{TIDE}-T_{NO_TIDE} averaged during the 30-year model run). During the cold phase of ENSO, the tide-induced changes in the current anomaly are not significant in either region east of Wenchang city or east of Qiongzhou Strait (Figures 12e and 12g). During the warm phase of ENSO, tides significantly enhance the northeastward current anomalies east of Wenchang city and weaken the eastward current anomalies around Qiongzhou Strait (Figure 12h). As a result, the temperature changes slightly during the cold phase (Figure 12e), whereas it significantly decreases during the warm phase in both regions east of Wenchang city and east of Qiongzhou Strait when tides are included in the model (Figure 12f).

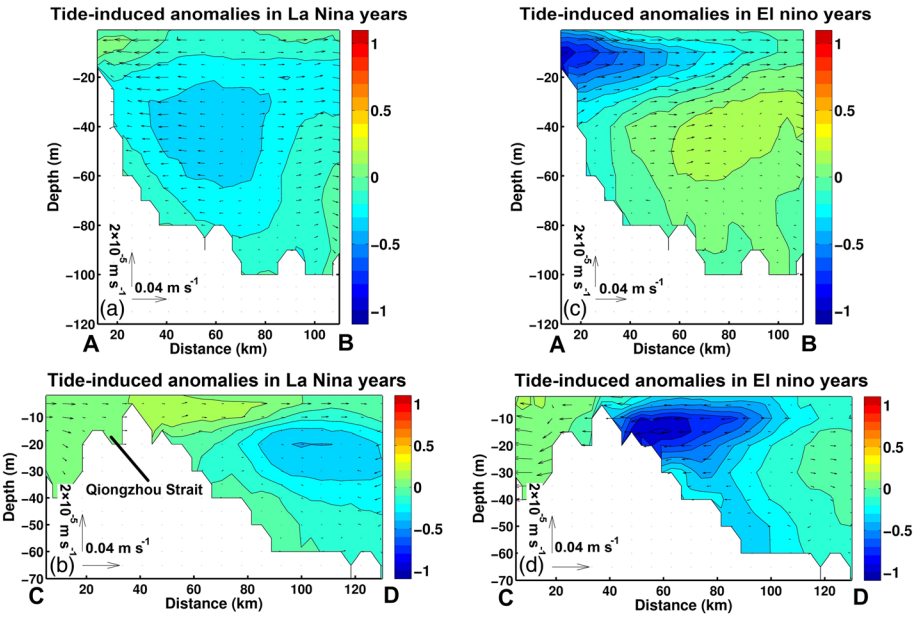

Figure 13. The differences of the monthly mean anomalies of sea temperature (color, units: °C) and currents (vectors) in July against climatology (30-year mean) between TIDE and NO_TIDE along (a, c) transect AB and (b, d) transect CD during the cold phase (La Niña, left panels) and warm phase (El Niño, right panels) of ENSO events.

Figure 13a further shows that tidal effects lead to anomalous onshore currents and sea temperature increases in the near surface in the coastal region of Wenchang city during the cold phase of ENSO. In addition, anomalous eastward currents east of Qiongzhou Strait bring warmer sea water into the region east of the strait (Figure 13b). During the warm phase, however, tidal effects lead to anomalous offshore currents, upwelling and a significant sea temperature decrease (over 1°C) in the coastal region of Wenchang city (Figure 13c), as well as anomalous westward currents east of the Qiongzhou Strait, which suppress the transport of warmer water from the strait and facilitate the compensation of cooler sea water from the surrounding regions (Figure 13d).

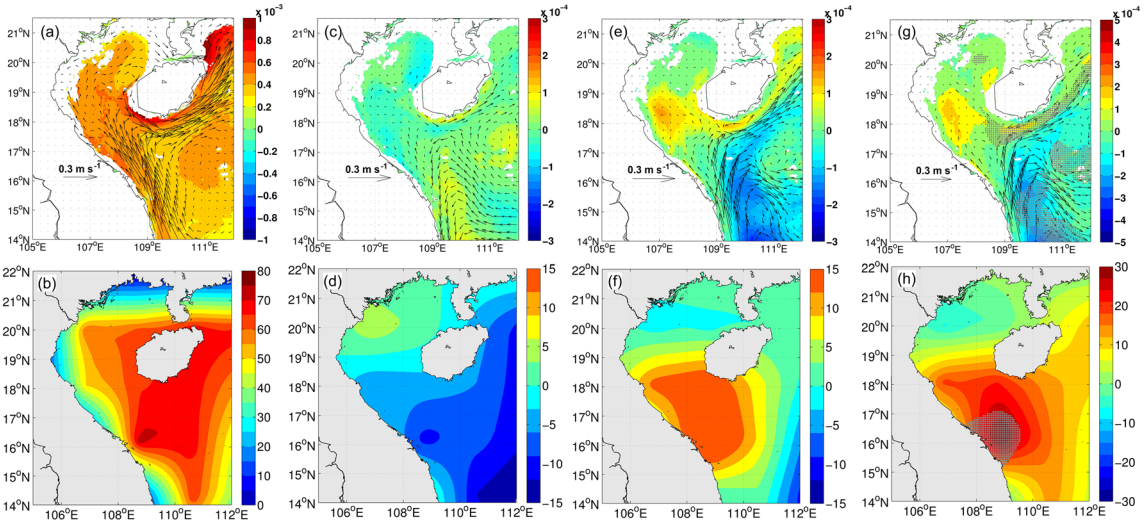

Figure 14. The climatology monthly mean of (a) buoyancy frequency (units: s^{-2}) between 10 and 30 m below the surface and (b) total heat flux (including the net heat flux and shortwave radiation, unit: W/m^2), their anomalies against climatology (30-year mean) in July for NO_TIDE during (c, d) the cold phase (La Niña) and (e, f) warm phase (El Niño) of ENSO events, and (g, h) the differences between warm phase and cold phase of ENSO events. Shaded area with dots indicates that differences between warm phase and cold phase of ENSO events are significant above the 95% confidence level.

As discussed in sections 3.2 and 3.3, stratification (background stratification without tidal mixing) in the upper ocean is essential to the tidal effects on the currents and subsurface water cooling in the regions in summer. Thus, we investigate the anomalies of stratification against the climatology when tides are excluded during different phases of ENSO events. Here the intensity of stratification is defined by the buoyancy frequency $N^2 = -\frac{g}{\rho_0}-\frac{\partial_\rho}{\partial_z}$. Figures 14a and 14b show that the ocean obtains heat in most regions around Hainan Island in July. In addition, the upper ocean stratification is affected by atmospheric forcing as well as the transport of water with stronger stratification from the coastal region of Vietnam around 14°N to 16°N. The upper ocean stratification is weaker than the climatology during the cold phase of ENSO, whereas it is much stronger during the warm phase (Figures 14c, 14e, and 14g) in most region around Hainan Island. The inhomogeneous tidal mixing under the condition of intensified stratification during the warm phase of ENSO changes the pressure gradient and thus the circulation, resulting in surface and subsurface sea water cooling in both regions east of Wenchang city and east of the Qiongzhou Strait.

Notably, the amplitudes of tides do not vary significantly on interannual scales. The interannual variations in tidal effects presented in this study are mainly due to the changes in ocean states (specifically, stratification) caused by large-scale air-sea interaction processes (Hu & Wang, 2016; Xie et al., 2003). As shown in Figures 14d and 14f, the total heat flux anomalies are positive (negative) during the warm (cold) phase of ENSO over most regions around the summer western boundary currents of the SCS (i.e., the strong northward and northeastward currents shown in Figures 3b, 3d, and 4b). Moreover, the magnitude of heat flux anomalies and boundary current anomalies during the warm phase of ENSO is much larger than that during the cold phase (Figures 14c–14f). As a result, the positive heat flux anomalies as well as stronger north or northeastward current anomalies significantly intensify the stratification of the coastal region around Hainan Island as well as the open ocean in the Beibu Gulf during the warm phase of ENSO. Under this condition, tides act as agents to mix subsurface and bottom waters in the shallow region, causing significant circulation changes in the northwestern SCS. Additionally, previous studies have found that the interactions between barotropic forcings, including geostrophic currents, wind-driven (Ekman) currents, and tidal currents in the bottom boundary layer could cause tidal variability on interannual and decadal scales, which is significantly correlated with mean sea level (Devlin et al., 2014, 2017, 2018). Here we emphasize the role of baroclinic effects (stratification and tidal mixing) induced by large-scale processes, such as air-sea interactions associated with different phases of ENSO events, on the interannual variations in tidal effects on the temperature, current, and sea level northeast of Hainan Island.

5. Conclusions

A high-resolution POM is used to investigate the tidal effects on the surface and subsurface cooling in the regions east of Wenchang city and east of the Qiongzhou Strait, northeast of Hainan Island, as detected by satellite SST images during summer. The following conclusions were obtained as a result of this study.

The results demonstrate that although tides significantly affect the currents in the northwestern SCS throughout the year, their impacts on the sea temperature are significant only during late spring and summer. Specifically, tides enhance the mixing rate in the coastal regions of the northwestern SCS, which generates a pressure gradient between near-shore and offshore regions during spring and summer. A dynamical analysis indicates that the anomalies of the pressure gradient induced by tidal mixing under strong stratification in summer around Hainan Island and Beibu Gulf are essential to both current changes and temperature reduction in the regions east of Wenchang city and east of Qiongzhou Strait (effects of remote tidal mixing). Specifically, the anomalous pressure gradient not only drives offshore currents in the coastal region of Wenchang city, which favors upwelling occurrence and causes sea temperature reduction, but also induces westward currents east of Qiongzhou Strait which suppress warm water transport from the strait and result in compensation for cold water from the surrounding regions.

The results from the temperature advection flux analysis further confirm that tide-induced upwelling is the main cause of sea water cooling east of Wenchang city. In addition, the local tidal mixing as well as the tide-induced prevention of warmer water transport from the Qiongzhou Strait accompanied by the compensation of cooler water from the surrounding regions are the primary causes of sea water cooling east of the Qiongzhou Strait.

In addition to the seasonal variations, the tidal effects on the surface and subsurface sea water cooling northeast of Hainan Island (east of Wenchang city and east of the Qiongzhou Strait) have interannual variations due to the changes in large-scale upper ocean states associated with different phases of ENSO events. During the warm phase (El Niño), the water cooling is significantly enhanced due to the intensified offshore currents and upwelling induced by tides along the eastern coast of Wenchang city. The tide-induced westward current anomalies are generated around the Qiongzhou Strait, resulting in stronger sea water cooling east of the strait. During the cold phase (La Niña), the above tide-induced anomalies are not significant in either region. Further analysis indicates that the interannual variations in tidal effects are mainly attributed to intensified (weakened) stratification by large-scale air-sea interaction processes during the warm (cold) phases of ENSO events.

Notably, the amplitudes of tides do not vary significantly on seasonal or interannual scales. The seasonal or interannual variations in the tidal effects presented in this study are mainly due to the changes in ocean states (specifically, background stratification without tidal forcings) caused by large-scale processes, such as atmospheric fluxes and circulation changes associated with different phases of ENSO events. As such, it would be interesting to investigate the connections between variations in upwellings in different coastal regions of the SCS, which will be addressed in future work.

Data Availability Statement

We are grateful for access to the following freely available data: sea surface temperature data of NASA/JPL available at ftp://podaac.jpl.nasa.gov/pub/sea_surface_temperature/avhrr/pathfinder/data_v5/; MODIS data of NASA available at https://oceandata.sci.gsfc.nasa.gov/MODIS-Aqua/; SODA data available at http://dsrs.atmos.umd.edu/DATA/soda3.3.1/ORIGINAL/ocean/; and the research quality data set of the Joint Archive for Sea level (JASL) available at ftp://ftp.soest.hawaii.edu/uhslc/rqds/pacific/ website.

Acknowledgments

This work was jointly supported by the Strategic Priority Research Program of the Chinese Academy of Sciences (grant XDA19060503), the Major Projects of the National Natural Science Foundation of China (grants 41890851 and 41931182), Key Special Project for Introduced Talents Team of Southern Marine Science and Engineering Guangdong Laboratory (Guangzhou, grant GML2019ZD0303), Guangdong Key Project (2019BT2H594), the National Science Foundation of China (grants 41776028 and 41676016), Innovation Research Group of National Natural Science Foundation of China (grant 41521005), Funding of China Scholarship Council (grant 201704910146), the Chinese Academy of Sciences (grants ZDRW-XH-2019-2, ISEE2018PY05, and 133244KYSB20180029), and the Independent Research Project Program of the State Key Laboratory of Tropical Oceanography (grant LTOZZ1902). The authors gratefully acknowledge the use of the HPCC at the South China Sea Institute of Oceanology, Chinese Academy of Sciences. This is contribution number 1959 of the NOAA Great Lakes Environmental Research Laboratory. We greatly appreciate Nicole Rice of NOAA GLELR for editing this paper. The views, opinions, and findings contained in this report are those of the authors and should not be construed as official NOAA or U. S. Government positions, policies, or decisions.

References

Atlas, R., Hoffman, R. N., Ardizzone, J., Leidner, S. M., Jusem, J. C., Smith, D. K., & Gombos, D. (2011). A cross-calibrated, multiplatform ocean surface wind velocity product for meteorological and oceanographic applications. *Bulletin of the American Meteorological Society*, *92*(2), 157–174. https://doi.org/10.1175/2010BAMS2946.1

Bai, P., Gu, Y. Z., Li, P. L., & Wu, K. J. (2016). Modelling the upwelling off the east Hainan Island coast in summer. *Chinese Journal of Oceanology and Limnology*, *34*(6), 1358–1373. https://doi.org/10.1007/s00343-016-5147-5

Bai, X., Wang, J., Sellinger, C., Clites, A., & Assel, R. (2012). Interannual variability of Great Lakes ice cover and its relationship to NAO and ENSO. *Journal of Geophysical Research*, *117*, C03002. https://doi.org/10.1029/2010JC006932

Bakun, A., Roy, C., & Lluch-Cota, S. E. (1998). Coastal up-welling and other ecosystem processes controlling the marine resource productivity of the western Indian Ocean. In *Status and Future of the Large Marine Ecosystems of the Indian Ocean* (pp. 103–141). Cambridge, MA: Blackwell Science.

Blumberg, A. F., & Mellor, G. L. (1987). A description of a three-dimensional coastal ocean circulation model. In N. S. Heaps (Ed.), *Three dimensional coastal ocean models* (pp. 1–16). Washington, D.C: American Geophysical Union. https://doi.org/10.1029/CO004p0001

Caldwell, P. C., Merrifield, M. A., & Thompson, P. R. (2015). Sea level measured by tide gauges from global oceans-the joint archive for sea level holdings (NCEI accession 0019568), Version 5.5, NOAA National Centers for Environmental Information, dataset, https://doi.org/10.7289/V5V40S7W

Carton, J. A., Chepurin, G. A., & Chen, L. (2018). SODA3: A new ocean climate reanalysis. *Journal of Climate*, *31*(17), 6967–6983. https://doi.org/10.1175/JCLI-D-18-0149.1

Chang, C.-W. J., Hsu, H.-H., Wu, C.-R., & Sheu, W.-J. (2008). Interannual mode of sea level in the South China Sea and the roles of El Niño and El Niño Modoki. *Geophysical Research Letters*, *35*, L03601. https://doi.org/10.1029/2007GL032562

Chia, F., Xie, H., & Shi, M. (2001). Upwelling east of Hainan Island. *Oceanography China*, *13*, 129–137. (in Chinese with an English abstract)

Devlin, A. T., Jay, D. A., Talke, S. A., & Zaron, E. D. (2014). Can tidal perturbations associated with sea level variations in the western Pacific Ocean be used to understand future effects of tidal evolution? *Ocean Dynamics*, *64*(8), 1093–1120. https://doi.org/10.1007/s10236-014-0741-6

Devlin, A. T., Jay, D. A., Zaron, E. D., Talke, S. A., Pan, J., & Lin, H. (2017). Tidal variability related to sea level variability in the Pacific Ocean. *Journal of Geophysical Research: Oceans*, *122*, 8445–8463. https://doi.org/10.1002/2017JC013165

Devlin, A. T., Zaron, E. D., Jay, D. A., Talke, S. A., & Pan, J. (2018). Seasonality of tides in Southeast Asian waters. *Journal of Physical Oceanography*, *48*(5), 1169–1190. https://doi.org/10.1175/JPO-D-17-0119.1

Egbert, G. D., & Erofeeva, S. Y. (2002). Efficient inverse modeling of barotropic Ocean tides. *Journal of Atmospheric and Oceanic Technology*, *19*(2), 183–204. https://doi.org/10.1175/1520-0426(2002)019<0183:EIMOBO>2.0.CO;2

Ekman, V. W. (1905). On the influence of the Earth's rotation on ocean currents. *Archives for Mathematics, Astronomy and Physics*, *2*(11), 1–52.

Fang, G., Chen, H., Wei, Z., Wang, Y., Wang, X., & Li, C. (2006). Trends and interannual variability of the South China Sea surface winds, surface height, and surface temperature in the recent decade. *Journal of Geophysical Research*, *111*, C11S16. https://doi.org/10.1029/2005JC003276

Guo, F., Shi, M., & Xia, Z. (1998). Diagnosis calculation of the east Hainan upwelling using a 2-D numerical model. *Acta Oceanologica Sinica*, *20*(6), 109–116. (in Chinese with an English abstract)

Hu, J., & Wang, X. H. (2016). Progress on upwelling studies in the China seas. *Reviews of Geophysics*, *54*, 653–673. https://doi.org/10.1002/2015RG000505

Jing, Z., Qi, Y., & Du, Y. (2011). Upwelling in the continental shelf of northern South China Sea associated with 1997–1998 El Nino. *Journal of Geophysical Research*, *116*, C02033. https://doi.org/10.1029/2010JC006598

Jing, Z., Qi, Y., Du, Y., Zhang, S., & Xie, L. (2015). Summer upwelling and thermal fronts in the northwestern South China Sea: Observational analysis of two mesoscale mapping surveys. *Journal of Geophysical Research: Oceans*, *120*, 1993–2006. https://doi.org/10.1002/2014JC010601

Jing, Z. Y., Qi, Y. Q., Hua, Z. L., & Zhang, H. (2009). Numerical study on the summer upwelling system in the northern continental shelf of the South China Sea. *Continental Shelf Research*, *29*(2), 467–478. https://doi.org/10.1016/j.csr.2008.11.008

Kalnay, E., Kanamitsu, M., Kistler, R., Collins, W., Deaven, D., Gandin, L., et al. (1996). The NCEP/NCAR 40-year reanalysis project. *Bulletin of the American Meteorological Society*, *77*(3), 437–471. https://doi.org/10.1175/1520-0477(1996)077<0437:TNYRP>2.0.CO;2

Kug, J. S., & Jin, F.-F. (2009). Two types of El Niño events: Cold tongue El Niño and warm pool El Niño. *Journal of Climate*, *22*(6), 1499–1515. https://doi.org/10.1175/2008JCLI2624.1

Laurent, S., Simmons, H. L., & Jayne, S. R. (2002). Estimating tidally driven mixing in the deep ocean. *Geophysical Research Letters*, *29*(23), 2106. https://doi.org/10.1029/2002GL015633

Li, Y., Peng, S., Wang, J., Yan, J., & Huang, H. (2018). On the mechanism of the generation and interannual variations of the summer upwellings west and southwest off the Hainan Island. *Journal of Geophysical Research: Oceans*, *123*, 8247–8263. https://doi.org/10.1029/2018JC014226

Li, Y., Peng, S., Yang, W., & Wang, D. (2012). Numerical simulation of the structure and variation of upwelling off the east coast of Hainan Island using QuikSCAT winds. *Chinese Journal of Oceanology and Limnology*, *30*(6), 1068–1081. https://doi.org/10.1007/s00343-012-1275-8

Lin, P. G., Cheng, P., Gan, J. P., & Hu, J. Y. (2016). Dynamics of wind-driven upwelling off the northeastern coast of Hainan Island. *Journal of Geophysical Research: Oceans*, *121*, 1160–1173. https://doi.org/10.1002/2015JC011000

Liu, Q. Y., Wang, D., Wang, X., Shu, Y., Xie, Q., & Chen, J. (2014). Thermal variations in the South China Sea associated with the eastern and central Pacific El Niño events and their mechanisms. *Journal of Geophysical Research: Oceans*, *119*, 8955–8972. https://doi.org/10.1002/2014JC010429

Locarnini, R. A., Mishonov, A. V., Antonov, J. I., Boyer, T. P., Garcia, H. E., Baranova, O. K., et al. (2013). In S. Levitus & A. Mishonov (Eds.), *World Ocean Atlas (2013), Volume 1: Temperature* (Vol. 73, p. 40). Silver Spring, MD: Technical Ed NOAA Atlas NESDIS.

Mellor, G. L. (2004). Users guide for a three-dimensional, primitive equation, numerical ocean model (June 2004 version). In *Prog. In Atmos. And ocean. Sci* (pp. 1–56). Princeton, NJ: Princeton Univ.

Mellor, G. L., & Yamada, T. (1982). Development of a turbulence closure model for geophysical fluid problems. *Reviews of Geophysics and Space Physics*, *20*(4), 851–875. https://doi.org/10.1029/RG020i004p00851

NASA Goddard Space Flight Center, Ocean Ecology Laboratory, Ocean Biology Processing Group. Moderate-resolution Imaging Spectroradiometer (MODIS) Aqua 11μm Day/Night Sea Surface Temperature Data (2014). Reprocessing. NASA OB.DAAC, Greenbelt, MD, USA. https://doi.org/10.5067/AQUA/MODIS/L2/SST/2014

Ren, H. L., & Jin, F. F. (2011). Niño indices for two types of ENSO. *Geophysical Research Letters*, *38*, L04704. https://doi.org/10.1029/2010GL046031

Shi, M., Chen, C., Xu, Q., Lin, H., Liu, G., Wang, H., et al. (2002). The role of the Qiongzhou Strait in the seasonal variation of the South China Sea circulation. *Journal of Physical Oceanography*, *32*(1), 103–121. https://doi.org/10.1175/1520-0485(2002)032<0103:TROQSI>2.0.CO;2

Song, X., Lai, Z., Ji, R., Chen, C., Zhang, J., Huang, L., et al. (2012). Summertime primary production in northwest South China Sea: Interaction of coastal eddy, upwelling and biological processes. *Continental Shelf Research*, *48*, 110–121. https://doi.org/10.1016/j.csr.2012.07.016

Su, J., & Pohlmann, T. (2009). Wind and topography influence on an upwelling system at the eastern Hainan coast. *Journal of Geophysical Research*, *114*, C06017. https://doi.org/10.1029/2008JC005018

Su, J., Wang, J., Pohlmann, T., & Xu, D. (2011). The influence of meteorological variation on the upwelling system off eastern Hainan during summer 2007–2008. *Ocean Dynamics*, *61*(6), 717–730. https://doi.org/10.1007/s10236-011-0404-9

Su, J., Xu, M., Pohlmann, T., Xu, D., & Wang, D. R. (2013). A western boundary upwelling system response to recent climate variation (1960–2006). *Continental Shelf Research*, *57*, 3–9. https://doi.org/10.1016/j.csr.2012.05.010

Su, J. L. (2004). Overview of the South China Sea circulation and its influence on the coastal physical oceanography outside the Pearl River Estuary. *Continental Shelf Research*, *24*(16), 1745–1760. https://doi.org/10.1016/j.csr.2004.06.005

Sun, J., Oey, L., Chang, R., Xu, F., & Huang, S.-M. (2015). Ocean response to typhoon Nuri (2008) in western Pacific and South China Sea. *Ocean Dynamics*, *65*(5), 735–749. https://doi.org/10.1007/s10236-015-0823-0

Wang, C., Wang, W., Wang, D., & Wang, Q. (2006). Interannual variability of the South China Sea associated with El Niño. *Journal of Geophysical Research*, *111*, C03023. https://doi.org/10.1029/2005JC003333

Wang, D., Yang, Y., Wang, J., & Bai, X. (2015). A modeling study of the effects of river runoff, tides, and surface wind-wave mixing on the Eastern and Western Hainan upwelling systems of the South China Sea, China. *Ocean Dynamics*, *65*(8), 1143–1164. https://doi.org/10.1007/s10236-015-0857-3

Wang, J. (1996). Global linear stability of the 2-D shallow water equations: An application of the distributive theorem of roots for polynomials on the unit circle. *Monthly Weather Review*, *24*(6), 1301–1310.

Wu, C.-R., Shaw, P.-T., & Chao, S.-Y (1998). Seasonal and interannual variations in the velocity field of the South China Sea. *Journal of Oceanography*, *54*, 361–372.

Wyrtki, K. (1961). Physical oceanography of the Southeast Asia waters. NAGA Report, 2: 1–195.

Xie, S. P., Xie, Q., Wang, D., & Liu, W. T. (2003). Summer upwelling in the South China Sea and its role in regional climate variations. *Journal of Geophysical Research*, *108*(C8), 3261. https://doi.org/10.1029/2003JC001867

Yang, H., & Wu, L. (2012). Trends of upper-layer circulation in the South China Sea during 1959-2008. *Journal of Geophysical Research*, *117*, C08037. https://doi.org/10.1029/2012JC008068

Yang, Y. L., Xie, S. P., Du, Y., & Tokinaga, H. (2015). Interdecadal difference of interannual variability characteristics of South China Sea SSTs associated with ENSO. *Journal of Climate*, *28*(18), 7145–7160. https://doi.org/10.1175/JCLI-D-15-0057.1

Yeh, S.-W., Kug, J.-S., Dewitte, B., Kwon, M.-H., Kirtiman, K. B. P., & Jin, F.-F. (2009). El Niño in a changing climate. *Nature*, *461*(7263), 511–514. https://doi.org/10.1038/nature08316

Yu, J.-Y., Zou, Y., Kim, S. T., & Lee, T. (2012). The changing impact of El Niño on US winter temperatures. *Geophysical Research Letters*, *39*, L15702. https://doi.org/10.1029/2012GL052483

Yu, W. (1987). A preliminary study of the upwelling system in the northern South China Sea. *Ocean Science*, *6*, 7–10. (in Chinese)

Zeng, X., Belkin, I. M., Peng, S., & Li, Y. (2014). East Hainan upwelling fronts detected by remote sensing and modelled in summer. *International Journal of Remote Sensing*, *35*(11–12), 4441–4451. https://doi.org/10.1080/01431161.2014.916443

Zhang, Y. C., & Qian, Y. F. (1999). Numerical simulation of the regional ocean circulation in the coastal area of China. *Advances in Atmospheric Sciences*, *16*(3), 443–450.

Zhu, X.-H., Ma, Y.-L., Guo, X., Fan, X., Long, Y., Yuan, Y., et al. (2014). Tidal and residual currents in the Qiongzhou Strait estimated from shipboard ADCP data using a modified tidal harmonic analysis method. *Journal of Geophysical Research: Oceans*, *119*, 8039–8060. https://doi.org/10.1002/2014JC009855

Zhu, X.-H., Zhu, Z.-N., Guo, X., Ma, Y.-L., Fan, X.-P., Dong, M., & Zhang, C. (2015). Measurement of tidal and residual currents and volume transport through the Qiongzhou Strait using coastal acoustic tomography. *Continental Shelf Research*, *108*, 65–75. https://doi.org/10.1016/j.csr.2015.08.016